Nanoscale

PAPER

Unbinding forces and energies between a siRNA molecule and a dendrimer measured by force spectroscopy

Cite this: DOI: 10.1039/c5nr04906g

Andra C. Dumitru,[a] Elena T. Herruzo,[a] Estrella Rausell,[b] Valentin Ceña[c] and Ricardo Garcia[a]

Received 22nd July 2015,
Accepted 3rd November 2015
DOI: 10.1039/c5nr04906g
www.rsc.org/nanoscale

We have measured the intermolecular forces between small interference RNA (siRNA) and polyamidoamine dendrimers at the single molecular level. A single molecule force spectroscopy approach has been developed to measure the unbinding forces and energies between a siRNA molecule and polyamidoamine dendrimers deposited on a mica surface in a buffer solution. We report three types of unbinding events which are characterized by forces and free unbinding energies, respectively, of 28 pN, 0.709 eV; 38 pN, 0.722 eV; and 50 pN, 0.724 eV. These events reflect different possible electrostatic interactions between the positive charges of one or two dendrimers and the negatively charged phosphate groups of a single siRNA. We have evidence of a high binding affinity of siRNA towards polyamidoamine dendrimers that leads to a 45% probability of measuring specific unbinding events.

Introduction

To address the role of proteins in cellular physiology or pathology requires an approach that should include the selective knocking down of such proteins to study the lack-of-function effect. Interference RNA technology and, more specifically, small interfering RNA (siRNA) has emerged as a very efficient and selective tool for this purpose since it induces sequence-specific degradation of target homologous single-stranded RNA[1] and it is able to inactivate a gene, and the expression of its encoded protein, at almost any stage in development.[2] However, major problems for siRNA intracellular delivery include poor cellular uptake from cell culture media, low siRNA stability and rapid clearance from the systemic circulation. A number of different siRNA delivery systems based on the combination of siRNA with nanoparticles (NPs) have been developed in order to overcome these problems.[3–6] One of the most promising uses of dendrimers is as NPs. Dendrimers are branched polymers with repetitive structures that have been widely exploited for their potential biological applications including siRNA delivery.[7–9] Polyamidoamine (PAMAM) dendrimers[10,11] have become the most widely used dendrimer-based vectors for gene transfer since the primary amines located on the surface of these dendrimers provide a high cationic charge density that favors siRNA binding through the phosphate backbone, forming a complex called dendriplex. However, the parameters that govern the efficiency of a given dendrimer to successfully deliver siRNA inside the cell are not well understood. In particular, it is important to understand the interaction forces that bind the dendrimer to the nucleic acid. Molecular modelling studies have shown that a very small force of interaction precludes the stability of the dendriplex while a strong interaction force prevents the intracellular dissociation of siRNA from the dendrimer and leads to the consequent failure of knocking down the target protein.[12]

Single molecule force spectroscopy (SFS) has been successfully applied to measure the forces between ligands and receptors,[13,14] antibody–antigen,[15–18] to investigate the unfolding of proteins,[19–22] protein stability,[23] the interaction between carbohydrates,[24] and cell adhesion.[25,26] In SFS experiments, the force dependence on the probe–surface distance (force curve) is recorded. A force curve could include sections where the force changes continuously with the distance and other sections that show step-like transitions (jumps). These jumps are associated with the rupture of the molecular bonds that were formed when the molecules attached to the tip came into contact with those deposited on the sample surface. The forces measured by SFS scale up with the loading rate[27–29] and could also be influenced by the electrostatic interactions[30] with the environment (pH, ionic concentration).

Despite the fact that a quantitative understanding of the interaction forces and energies between nucleic acids and nanoparticles used in gene delivery systems is of great impor-

[a]Instituto de Ciencia de Materiales de Madrid, CSIC, c/Sor Juana Ines de la Cruz 3, 28049 Madrid, Spain
[b]Departamento de Anatomía, Histología y Neurociencia, Facultad de Medicina, Universidad Autónoma de Madrid, Madrid, Spain
[c]Unidad Asociada Neurodeath, Facultad de Medicina, UCLM and CIBERNED, ISCIII, Albacete, Spain

tance for optimizing the transfection efficiency, only a few studies have focused on this matter. Xu *et al.* have investigated the interaction forces between chitosan molecules and siRNA as a function of the media pH.[31]

Here, a single molecule force spectroscopy approach is developed to measure the unbinding forces and free energies between siRNA and PAMAM dendrimers at the single molecular level. The formation of dendriplexes (siRNA–dendrimer complex) has been quantified in terms of affinity and stability of the formed complex. We provide evidence of a high binding affinity of siRNA towards dendrimer nanoparticles, with a binding probability of up to 45%. At a loading rate of 1 nN s^{-1}, we find three different values of the unbinding force, 28 pN ± 6 pN, 38 ± 8 pN and 50 ± 9 pN. These forces reflect three different siRNA–dendrimer interaction configurations characterized by free unbinding energies of 0.709 ± 0.01 eV (16.34 ± 0.23 kcal mol^{-1}), 0.722 ± 0.012 eV (16.49 ± 0.28 kcal mol^{-1}) and 0.724 ± 0.011 eV (16.69 ± 0.25 kcal mol^{-1}), respectively. The configurations with free energies of 0.722 eV and 0.724 eV are associated with complex lifetimes of 5 ± 2 s and energy barrier lengths of 0.14 ± 0.03 nm while the configuration with a free energy of 0.709 eV has a lifetime of 3 ± 1 s and a barrier length of 0.25 ± 0.06 nm.

Since largely ramified dendrimers lead to significant toxicity *in vivo*,[32] we have chosen the highly biocompatible G1 TRANSGENE PAMAM (G1 TGD PAMAM) dendrimer because of its negligible toxicity and its ability to efficiently deliver siRNA and to induce gene silencing in primary neuronal cultures.[33,34] This dendrimer represents a good model to study the single molecule interaction between dendrimers and siRNA including the binding forces involved in such an interaction. A better knowledge of this interaction will help in the design of more efficient dendrimers to deliver siRNA to the target cells.

Experimental methods

Materials and reagents

Phosphate buffered solution (PBS), 4-(2-hydroxyethyl)-1-piperazineethanesulfonic acid (HEPES), hydrogen peroxide 30%, sulphuric acid, 3-aminopropyl-triethoxysilane (APTES), glutaraldehyde 8%, 6-aminohexanethiol, ethanol and dimethyl sulfoxide (DMSO) were purchased from Sigma Aldrich (Spain). 24-unit ethylene glycol functionalized with succinimidyl and maleimido ends (NHS-PEG_{24}-Mal) was purchased from Fisher Scientific (Spain).

The G1 TGD PAMAM dendrimer combining a conjugated rigid polyphenylenevinylene (PPV) core with flexible polyamidoamine (PAMAM) branches was synthesized as previously described.[35] Thiol-functionalized siRNA, diethylpyrocarbonate (DEPC) and heparin were obtained from Sigma Aldrich (Spain).

Tip functionalization

Triangular silicon nitride cantilevers were first aminofunctionalized as described previously.[36] Briefly, they were cleaned thoroughly by immersion in a piranha solution (4 volumes of an aqueous solution of 70% sulfuric acid with 1 volume of a solution of 30% hydrogen peroxide) for 30 minutes. The cantilevers were then rinsed with ultrapure water and dipped into a solution of APTES : water : ethanol (volume ratio 5 : 5 : 90) for 45 minutes. Finally, the amino-functionalized tips were rinsed with ultrapure water and ethanol and dried with nitrogen gas. Next, the heterobifunctional NHS-PEG_{24}-Mal linker was dissolved in PBS to a concentration of 1 mM. The APTES-functionalized AFM tips were immersed into the PEG linker solution for 30 minutes at room temperature.

Finally, the AFM tips functionalized with the PEG linker were immersed into a 2.5 μM siRNA solution for 12 hours at room temperature.[37] The tips were then rinsed with 10 mM HEPES and stored in a Petri dish at 4 °C until further use.

Dendrimer deposition

After a 30 minute ultrasonic treatment to prevent dendrimer aggregation, 20 μl of a 100 μM dendrimer solution was deposited onto a freshly cleaved piece of mica for 2 minutes. The sample was then rinsed with 10 mM HEPES.

Single molecule force spectroscopy measurements

Single molecule force spectroscopy experiments were performed at room temperature with a Cypher microscope (Asylum Research, Santa Barbara, USA). The experiments were performed in 0.1 M phosphate buffered solution (PBS) at pH 7.4. Triangular silicon nitride cantilevers (MSCT, Bruker, Santa Barbara, USA) with a nominal spring constant of 0.01 N m^{-1} and a resonant frequency of 7 kHz were used. The force spectroscopy measurements involve the accurate determination of the cantilever force constant as well as the optical lever sensitivity. The force constant and quality factor are determined by using the thermal noise method.[38,39] The calibrated force constant of the cantilevers was 0.02 ± 0.002 N m^{-1}. At the end of each experiment, the optical lever sensitivity was calibrated by acquiring deflection *versus* distance curves on a hard surface (mica). Typically 100 deflection *versus* distance curves were acquired and the sensitivity of the photodiode was calculated as the mean value of the slope of the deflection curve measured in the repulsive region. The force was calculated by using Hooke's law, $F = -k\Delta z$ (Δz is the cantilever deflection, k is the cantilever force constant). The maximum force was maintained below 150 pN to avoid damaging the molecules bound to the tip apex. The force curves were acquired by approaching and retracting the tip 100 nm from the sample at different velocities (from 100 nm s^{-1} to 2.5 μm s^{-1}). In each curve, the tip was kept in contact with the sample for 0.5 s to facilitate the formation of siRNA–dendrimer complexes. For each functionalized tip, we have acquired several force maps, where a force curve was recorded as a function of the (x, y) coordinate. These force maps covered 1 μm × 1 μm regions (32 × 32 data points).

Force spectroscopy data analysis

A total of 16 000 force distance curves were analysed by using customized software. The curves were averaged and the contact

point was set by establishing a deflection threshold. The detection of an adhesion force event (either specific or unspecific) was based on the values of the second and third derivatives of the deflection. The event was labeled as an adhesion event whenever the above derivatives were found to be above 20% with respect to the noise level. An algorithm was created to discriminate unspecific from specific adhesion events between siRNA and dendrimers. First, the slope of the adhesion event (force *versus* piezo displacement) near the jump-off point is calculated. Then tables containing information on adhesion events for all the experiments are processed. We generated two types of representations: a common plot showing the number of events with a given unbinding force (1D histogram) and plots showing the number of events with a given unbinding force and a given value of another parameter, for example, the unbinding length (2D histograms). To discriminate between specific and unspecific binding events we gathered a series of 2D histograms. In these histograms, the *y*-axis represents the unbinding force and the *x*-axis could be the binding distance or the slope of an adhesion event. The 2D histograms show several spots above the average values. To ascribe one of these spots to a specific or an unspecific event we introduced several phenomenological observations. Unspecific adhesion events are usually found near the solid support (retraction curve), here at tip–surface separations below 5 nm. In addition, the characteristic slope in the force curve of an unspecific event is steeper than the one corresponding to a specific siRNA–dendrimer interaction. The application of the above criteria to the 2D histograms enables the removal of the spots associated with unspecific interactions from the plots leaving what we call a 2D molecular recognition map. The use of 2D histograms is uncommon in force spectroscopy, although it has been used as an alternative method to present the data.[40–42]

siRNA release by polyanion competition

The ability of the complexes to release siRNA in the presence of polyanionic heparin was determined as a measure of complex stability.[33] Complexes were prepared at a dendrimer/siRNA molar ratio of 10 to ensure the complete binding of siRNA by the dendrimer, and then incubated with varying concentrations of heparin sulfate (0.01, 0.02, 0.05, 0.1, 0.2 and 0.5 heparin USP units per mL) for 20 min. The solutions were loaded on a 1.2% (w/v) agar gel containing 0.05 mg ml^{-1} ethidium bromide. Electrophoresis was performed at 60 mV for 15 min, and the resulting gels were photographed under UV-illumination.

Control experiments

Several rounds of control experiments have been performed to check the specificity of the unbinding events. For the heparin competition assay, 0.2 heparin USP units per mL were injected into the siRNA–dendrimer solution and after 30 minutes molecular recognition events were recorded with a siRNA-functionalized tip. Another control experiment involved the measurement of force curves by using bare AFM tips on dendrimer monolayers deposited on mica. An additional control experiment involved the recording of force curves with siRNA-functionalized tips on a bare mica substrate.

Results and discussion

To perform the single molecule force spectroscopy measurements, the AFM tip is functionalized with a polyethylene glycol linker (PEG)–siRNA complex. Then, the functionalized tip is brought into contact with a packed dendrimer layer deposited onto the mica substrate (Fig. 1a). Fig. 1b shows the scheme of a force–distance plot (force curve) with four different steps. In step 1 the tip is far from the sample surface and the interaction force is non-existent; step 2 depicts the contact between the tip and the deposited molecules; step 3 depicts the repulsive forces between the tip and the sample when the tip is pushed toward the surface while in contact. In step 4, the tip is retracted (blue line) and the presence of an adhesion force will bend the tip downwards. The adhesion force could come from a specific molecular recognition event or from unspecific electrostatic interactions. Fig. 1b depicts a specific event. In fact a key point of SFS is to discriminate specific and unspecific interactions (see below). When the force gradient of the siRNA–dendrimer interaction exceeds the force constant value of the cantilever, the tip jumps out of contact to its initial position. The unbinding force (F_{unb}) of the siRNA–dendrimer pair is calculated from the vertical difference between the baseline and the minimum force at retraction. The unbinding length (L_{unb}) is the difference between the tip–sample distance where the unbinding event occurs and the contact point.

Detection of siRNA–dendrimer interactions

We have taken a total number of 16 000 force curves with 5 siRNA-functionalized tips on a packed dendrimer surface. The unbinding forces were extracted by recording force volume maps in different locations of the sample. Each force volume consisted of 32 × 32 force curves taken over a 1 μm × 1 μm area.

Fig. 2a shows several examples of the retraction part of the force *versus* distance curves obtained during the data acquisition process. The nonlinear stretching of the PEG tether before the cantilever jumps out of contact can be observed in all of the curves used in our analysis. The unbinding events were characterized by their unbinding length and unbinding force. In the Experimental methods section we introduce a procedure to identify and discriminate specific from non-specific interaction events.

Fig. 2b depicts the 1D histogram of the unbinding forces of specific siRNA–dendrimer interactions at a loading rate of 1 nN s^{-1}. A total of 1341 unbinding events are included in this plot. Unspecific or noisy events occurring at $F_{unb} \leq 15$ pN have been filtered out from this analysis. In this representation, the most frequent unbinding event is observed at $F_{unb} \approx 28$ pN. The positive skew of the histogram is an indication that multiple unbinding events occur.[43] However given the lower prob-

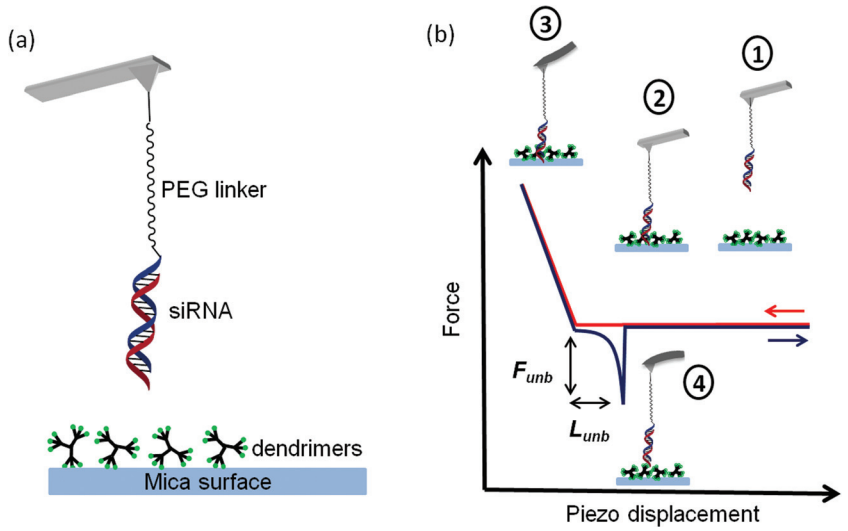

Fig. 1 (a) Scheme of the tip functionalization and dendrimer adsorption on mica. (b) Main steps of a force curve depicting a molecular recognition (specific) event. 1. Tip far from the surface. 2. Initial tip–surface contact (approaching). 3. Tip–surface repulsive region. 4. Molecular recognition unbinding force.

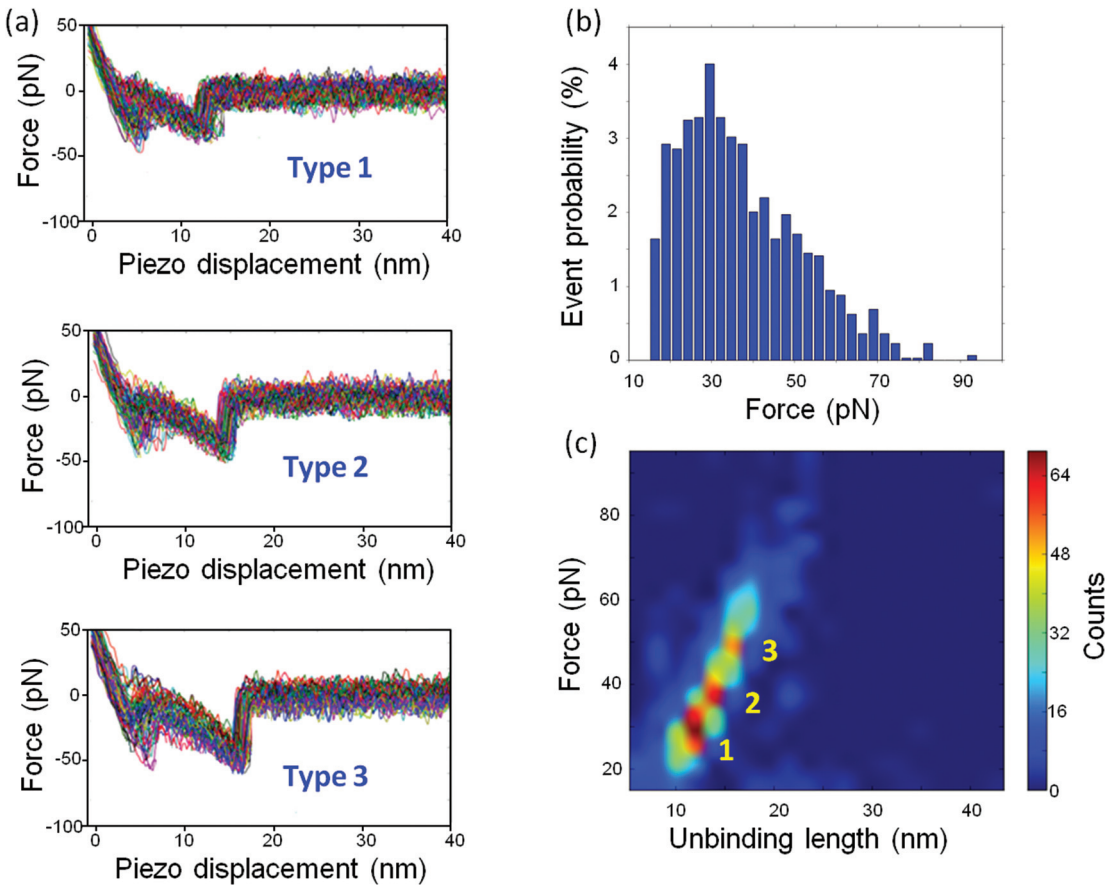

Fig. 2 (a) Force curves depicting specific siRNA–dendrimer unbinding events. The peak number is associated with the numbers shown in (c). (b) Histogram of the specific siRNA–dendrimer interactions at a loading rate of 1 nN s^{-1}. The histogram involves 1341 events. Only force curves representing specific events are included. (c) Two dimensional molecular recognition map. The map represents the events with the same force and unbinding distance.

ability of this kind of events, it is hard to determine the unbinding forces corresponding to multiple events.

Fig. 2c shows the 2D molecular recognition map containing the specific unbinding events with a given unbinding force and unbinding length. The events are plotted on a color-coded scale, where red and blue represent, respectively, the highest and the lowest number of events.

The observed unbinding forces can be grouped into three regions which are characterized, respectively, by maximum values of 28 ± 6 pN, 38 ± 8 pN and 50 ± 9 pN (at a force loading rate of 1 nN s^{-1}). In all the cases, the unbinding lengths are determined in the 10–17 nm range. By correlating the unbinding force and unbinding length, we observe that the events corresponding to the lowest force (28 pN) have shorter L_{unb} values (12 nm), while the events observed at higher forces (38 pN and 50 pN) have unbinding lengths, respectively, of 14 nm and 16 nm. The three different force curve signatures shown in Fig. 2a can be correlated with the regions 1, 2 and 3 of the 2D molecular recognition map. Similar results in terms of unbinding forces and lengths have been obtained with other siRNA-functionalized AFM tips.

The three peaks underline the presence of three-different interactions between siRNA and the dendrimers. The persistence length of a double stranded RNA molecule is about 70 nm.[44,45] This length is several times larger than the nominal siRNA length (5.9 nm), consequently, the siRNA will behave as a rigid rod. A comparison of the nominal length of the siRNA and the dendrimer size indicates that the siRNA molecule could interact simultaneously with several dendrimers.

Fig. 3 shows a model of the possible siRNA–dendrimer complexes consistent with our observations. In this context, the lower force peak will correspond to a configuration that minimizes the interaction between the siRNA and the dendrimers (Fig. 3a). Fig. 3b shows an intermediate configuration where the siRNA interacts partially with two dendrimers. A larger force peak (50 pN) implies that the siRNA lies flat on top of several dendrimer molecules (Fig. 3c). This configuration maximizes the electrostatic attractive interaction between the siRNA and the dendrimers.

We have performed three different sets of control experiments to determine the specificity of the measured binding events. Fig. 4 illustrates the typical force curves of the different control experiments. To emphasize the differences between specific and unspecific interactions, we also include a force curve with a siRNA functionalized tip and a dendrimer sample (Fig. 4a). In the first control experiment we have blocked the positively charged regions of the dendrimer by introducing heparin in the solution (Fig. 4b). In the second control, we have used unfunctionalized AFM tips (Fig. 4c). Finally we have also recorded force curves with a siRNA-functionalized tip on bare mica (Fig. 4d).

Heparin is a highly sulfated glycosaminoglycan that has the highest negative charge density of any known biological molecule.[46] It is expected to block most of the dendrimer's surface positive charges that are not bound to the mica. Heparin competition assays were performed in order to test the strength of

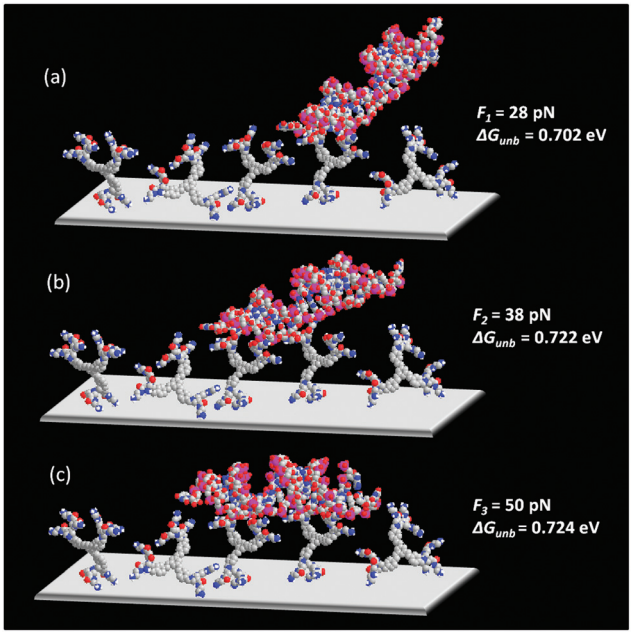

Fig. 3 Scheme of the dominant siRNA–dendrimer configurations on a mica surface as deduced from the data. The gray plane represents the position of the mica surface. (a) Lower force configuration that minimizes the electrostatic interaction between siRNA and the dendrimers; (b) intermediate configuration; (c) higher force configuration of a siRNA lying flat on top of two dendrimer molecules. This configuration increases the electrostatic attractive interaction between the siRNA and the dendrimers.

the union between the siRNA and the dendrimers.[12] Gel electrophoresis (Fig. 5a) shows that 1 μM dendrimer completely binds 100 nM siRNA (dendriplexes) and this is markedly displaced from its binding to the dendrimer by 0.2 United States Pharmacopeia (USP) heparin units per mL. This test was adapted for our single molecule force spectroscopy setup. Initially, molecular recognition events were recorded between a siRNA-functionalized AFM tip and dendrimers on the surface, then heparin was injected into the system and after 30 minutes molecular recognition events were recorded again.

Fig. 5b shows the unbinding force distributions before and after the introduction of heparin. The injection of a competing polyanion (heparin) into the medium leads to a significant reduction of the unbinding events. This is in good agreement with the experiment performed in bulk solution (Fig. 5a). In the absence of heparin, the probability of finding a force curve with the signature of a specific siRNA–TGD PAMAM dendrimer event is 45%. After heparin deposition, the probability is reduced to 11.6%. However, the distribution of the unbinding forces remains unchanged, with the most frequent unbinding events occurring at 28 pN. This is an indication that the remaining events have the same features as the initial ones, which is consistent with some residual activity between siRNA and dendrimers after heparin blocking.

We performed two additional control experiments. One involved the use of a non-functionalized AFM tip and dendri-

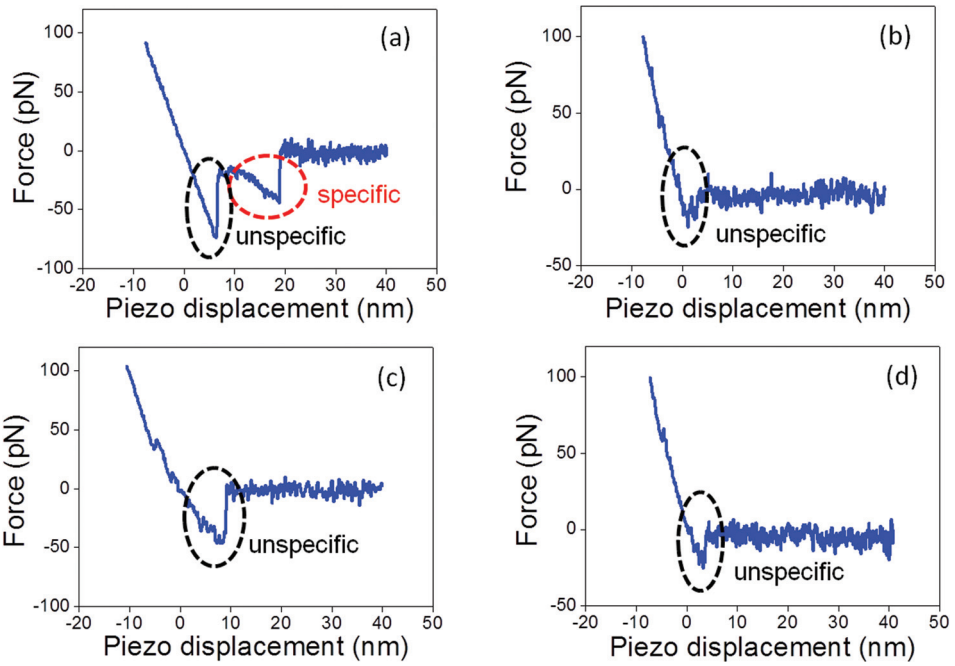

Fig. 4 Typical force curves for specific and unspecific unbinding events (a) signature of a specific siRNA–dendrimer unbinding event (circle). (b) Force curve between a siRNA-functionalized AFM tip and a dendrimer in the presence of heparin. (c) Force curve between a bare AFM tip and a dendrimer. (d) Force curve between a siRNA-functionalized tip and a bare mica surface.

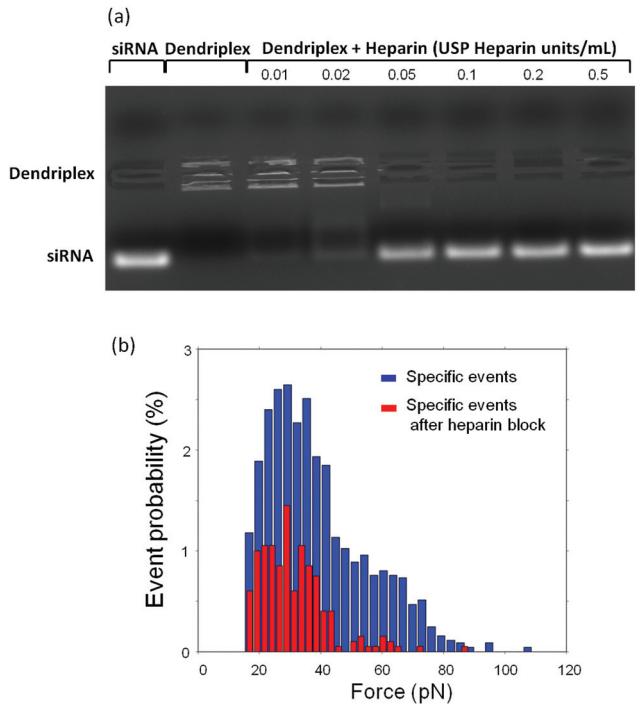

Fig. 5 (a) Gel electrophoresis plot. Displacement of siRNA (100 nM) bound to the G1 TGD dendrimer (1 μM) by increasing heparin concentrations (0.01 to 0.5 USP units per mL) in bulk solution. (b) Histograms of siRNA–dendrimer forces with and without the presence of heparin. Heparin binds to the dendrimers and dissociates the siRNA–dendrimer complex. Total number of events, respectively, before and after the introduction of heparin are 1263 and 209.

mers deposited on mica. In the other a siRNA-functionalized AFM tip recorded force curves on a bare mica surface. In both cases, the corresponding force curves did not provide any unbinding events with the signature used to characterize siRNA–dendrimer specific interactions.

Fit with the FJC model

In order to perform a quantitative analysis of the siRNA–PEG stretching before jump-out to the surface (step 4 in Fig. 1b), the specific unbinding events were fitted with the extended freely jointed chain (FJC) model (Fig. 6a). This model provides a quantitative description of the behaviour of a polymer under stretching[47,48]

$$L(F) = L_c(F)\left[\coth\left(\frac{Fl_p}{k_BT}\right) - \frac{k_BT}{Fl_p}\right] \quad (1)$$

where L is the molecular extension under force, F the applied force, l_p the persistence length (l_p = 0.35 nm for the PEG used here), T = 298 K, k_B the Boltzmann constant and L_c the contour length of the polymer (the polymer end-to-end distance under application of the force F).

The experimental nonlinear stretching of the force as a function of piezo-displacement was fitted to eqn (1) and the corresponding contour length of the siRNA–PEG complex was extracted. The fit to the FJC model renders a single-mode distribution of the most probable contour length centered at 17 ± 8 nm (Fig. 6b). This value is very close to the sum of the nominal contour length of the PEG linker used in these experi-

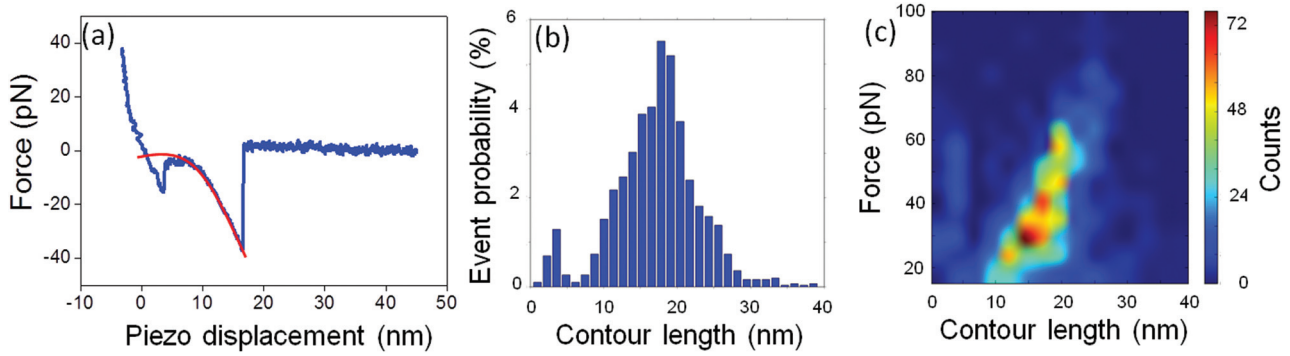

Fig. 6 (a) Typical unbinding force curve between a siRNA and a dendrimer. In red is the fitting with the freely-joined chain model. (b) Histogram of the unbinding events as a function of freely-joined contour length. The maximum happens at 16 nm which matches the sum of the nominal length of the PEG (10 nm) and the siRNA (6 nm). Total number of events 1341. (c) Two dimensional molecular recognition map of unbinding forces *versus* contour length of the siRNA and the PEG linker. The contour length is obtained by using the freely joined chain model.

ments 10 ± 5 nm (ref. 49,50) and the 21-base pair siRNA 5.9 nm (2.8 Å per base pair). Thus the value of the most probable contour length is in good agreement with the length corresponding to the PEG-linker/siRNA complex. Fig. 6c shows the 2D molecular recognition map of unbinding forces *versus* the contour length of the PEG-linker/siRNA complex. Only single-force events are included in this map. We can observe that there are three different regions in the 2D map, as follows: region 1 with F_{unb} = 28 pN and L_{c1} = 15 nm, region 2 with F_{unb} = 40 pN and L_{c2} = 17 nm and region 3 with F_{unb} = 58 pN and L_{c3} = 19 nm. The higher-force regions can be linked to multiple unbinding events. As for the contour lengths, we observe that $L_{c1} < L_{c2} < L_{c3}$. This behavior is at odds with the one observed by Sulchek *et al.*[51] for the stretching of multiple PEG tethers in parallel. Their fit by the FJC model for single and multiple bonds rendered $L_{c\ multiple} < L_{c\ single}$. On the other hand, it has been estimated that N, the largest number of bonds during a tip–sample contact, is approximately equal to the ratio of the surface area of the AFM tip spherical cap divided by the area occupied by one molecule,[52]

$$N = \frac{2R}{L_c} \tag{2}$$

where R is the tip radius and L_c is the contour length of the molecule bound to the tip. In our system the nominal tip radius is R = 10 nm and the calculated contour length L_c = 17 nm, which makes $N \approx 1$. Therefore, we conclude that in the present experiments it would be very difficult to have two or more siRNA molecules interacting simultaneously with the dendrimers.

Force spectroscopy at different loading rates

To determine the binding parameters of the siRNA–dendrimer complex and to gain insight into the energy landscape of the complex, we have carried out experiments at different loading rates. The kinetic model proposed by Bell[53] and further developed by Evans and Ritchie[27,28,54] predicts that the force of a single-energy barrier in a thermally activated regime scales up with the logarithm of the force loading rate,

$$F^* = \frac{k_B T}{x_\beta} \ln\left(\frac{\nu x_\beta}{k_{off} k_B T}\right) \tag{3}$$

here F^* is the most probable unbinding force, ν is the loading rate, x_β is the effective width of the energy barrier along the reaction coordinate, k_{off} is the dissociation rate of the bond at zero force and k_BT is the thermal energy. The effective loading rate was obtained by multiplying the tip pulling velocity with the effective force constant of the cantilever–PEG system. The effective force constant of the cantilever–PEG is equivalent to the force constant of two springs in series. A practical determination of the effective constant is obtained from the slope of the retraction curve before the jump-off to the surface.[27,54,55] The measured effective force constants were in the range of 3–3.7 pN nm^{-1}.

For each loading rate, the most probable unbinding force has been obtained from the maximum of the corresponding unbinding event histogram. Since we observe three different types of force curves in our experiments, we have followed the evolution of the most probable unbinding force with the loading rate for each type of force curve.

Fig. 7 shows the dependence of the most probable unbinding force *versus* the logarithm of the effective loading rate for the unbinding events corresponding to regions 1, 2 and 3 in Fig. 2a. The results are consistent with the prediction of eqn (3). The dynamic force spectrum shows a linear behaviour for all regions. We conclude that a single energy barrier characterizes the transition of the dendriplex from the bound to the unbound state.

The length of the energy barrier x_β was determined from the slope of the linear fit of the unbinding forces *versus* the loading rate logarithm plot. Next, k_{off} was calculated by extrapolation to zero forces. The characteristic time needed for the spontaneous dissociation of the siRNA–dendrimer complex, τ, is given by the inverse of the kinetic off-rate constant. This parameter can be correlated with the stability of the complex.

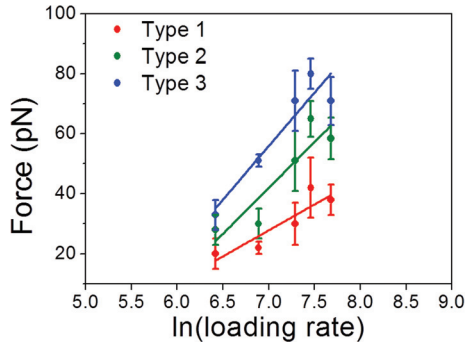

Fig. 7 Dependence of the unbinding force on the loading range (semilog plot). The Bell–Evans model has been used to obtain the plot.

The dissociation of the siRNA–dendrimer complex under an external force can be described in the frame of the transition state theory.[27,56] Once k_{off} is estimated using the Bell–Evans model, the measured free energy of the unbinding process ΔG_m can be calculated using the following equation, where h is the Planck's constant,

$$\Delta G_m = -k_B T \ln \frac{k_{off} h}{k_B T} \quad (4)$$

We consider that the siRNA–dendrimer system studied here meets the assumptions of the Eyring model due to the small number of bonds involved. The total number of positive charges present on the surface of a G1 TGD PAMAM dendrimer at neutral pH (pH ≈ 7.4) is 9 or three charges per branch. The dendrimers form a layer on mica which implies that at least one branch (three positive charges) will interact with the negatively charged mica substrate. Therefore, the maximum number of positive charges in a dendrimer available for interacting electrostatically with the negatively charged phosphate groups of the nucleic acid is 6. We also assume that the dissociation of the siRNA–dendrimer complex under force proceeds along a trajectory that resembles a thermodynamically favoured path, so the contribution of the entropic term can be neglected and the free energy change coincides with the change in enthalpy.

It must be noted that the above free energy includes the contribution of the siRNA–dendrimer complex unbinding $\Delta G_{complex}$ as well as of the PEG linker stretching ΔG_{PEG}. Hence, the unbinding free energy linked exclusively to the dissociation process between the siRNA and the dendrimer can be calculated as follows:

$$\Delta G_{complex} = \Delta G_m - \Delta G_{PEG} \quad (5)$$

The free energy related to the stretching of a 10 nm long PEG linker has been estimated experimentally to be −1.78 kcal mol^{-1}.[48] The unbinding free energies for the different siRNA–dendrimer configurations measured here are determined by using eqn (4) and (5). Table 1 summarizes the kinetic parameters–energy barrier bond length, intrinsic unbinding rate, bond lifetime and free energy of the bond for the three types of unbinding events introduced in Fig. 2a.

Table 1 Kinetic parameters of the molecular recognition process for the three types of unbinding events. The length of the energy barrier, x_β; the intrinsic unbinding rate of the bond, k_{off}; the characteristic time needed for the spontaneous dissociation of the siRNA–dendrimer complex, τ; the free unbinding energy, ΔG_{unb}

Force (pN)	x_β (nm)	k_{off} (s^{-1})	τ (s)	ΔG_{unb} (eV kcal^{-1} mol^{-1})
28	0.25 ± 0.06	0.32 ± 0.13	3.12 ± 1.17	0.709 ± 0.01/ 16.34 ± 0.23
38	0.14 ± 0.033	0.19 ± 0.09	5.39 ± 2.57	0.722 ± 0.012/ 16.49 ± 0.28
50	0.14 ± 0.028	0.18 ± 0.07	5.57 ± 2.11	0.724 ± 0.011/ 16.69 ± 0.25

The length of a hydrogen bond formed between a nitrogen donor and an oxygen acceptor lies between 0.15 and 0.25 nm, which is in good agreement with the energy barrier bond lengths obtained here. The complexes corresponding to lower unbinding forces (region 1 in Fig. 2a) are characterized by a barrier bond length of 0.25 ± 0.06 nm while the ones giving higher forces (regions 2 and 3 in Fig. 2a) show a smaller barrier bond length (0.14 ± 0.08 nm). A higher lifetime of 5.4 ± 2 s for the siRNA–dendrimer complexes corresponding to regions 2 and 3 implies a higher stability of these complexes as compared to the ones characterized by smaller unbinding forces. The latter will dissociate faster.

Molecular dynamics simulations show that the binding energies between the positive residues of the first-generation dendrimer and siRNA can be grouped in two clusters, 11.3–13.6 kcal mol^{-1} and 5.7–7.6 kcal mol^{-1}.[12] The spatial orientation of the residue with respect to the siRNA determines its value. The free unbinding energies measured here (16.34–16.69 kcal mol^{-1}) indicate a combination of a higher-energy and a lower energy residue (10.3 + 6.2 = 16.5 kcal mol^{-1}) as given by the simulations. The good agreement between the experimental results and the simulations strengthens the relevance of the simulations. Interestingly, although the unbinding free energies suggest that the number of electrostatic interactions involved in dendriplex formation is similar for all complexes, the spatial conformation of the interacting residues determines the stability of the formed complex.

Conclusion

We have developed a single molecule force spectroscopy method to measure the unbinding forces and energies between a single siRNA molecule and polyamidoamine dendrimers deposited on a mica surface. We report three types of unbinding events which are characterized, respectively, by forces and free unbinding energies of 28 pN (0.709 eV), 38 pN (0.722 eV) and 50 pN (0.724 eV). The probability of finding specific unbinding events is about 45%. This value reveals a

high binding affinity of siRNA towards polyamidoamine dendrimers. We propose that siRNA interacts either with two of the three amino branches of one dendrimer or with two branches of adjacent dendrimers. The specific binding interaction at 0.724 eV indicates that the siRNA lies flat on top of two dendrimer molecules. This configuration maximizes the electrostatic attractive interactions between the siRNA and the dendrimers. The lower peak corresponds to a configuration that minimizes the siRNA–dendrimer interactions. Intermediate configurations are also possible (0.722 eV). We provide relevant information for future PAMAM-type dendrimer synthesis aiming to achieve transfection procedures in two ways: (a) the binding forces between the amino terminal groups located in the PAMAM branches and the phosphate groups in the siRNA molecules should be in the range of 25 to 50 pN for loading rates of about 1 nN s^{-1} to allow the dissociation of the siRNA from the dendriplex and an efficient transfection at the same time; it protects the dendrimer from RNAse-mediated degradation and (b) it validates experimentally, for the first time, the theoretical predictions made by molecular modelling about the binding energies between dendrimers and siRNA at the single molecule scale.

Acknowledgements

This work was funded by the European Research Council ERC-AdG-340177 (3DNanoMech) grant to RG and by the Spanish Ministry of Economy (MINECO) through grants CSD2010-00024, MAT2013-44858-R to RG and BFU2011-30161-C02-01 and BFU2014-59009-P to VC.

References

1 C. Curtis and A. Nardulli, in *The Nuclear Receptor Superfamily*, ed. I. McEwan, Humana Press, 2009, vol. 505, ch. 11, pp. 187–204.
2 F. Pérez-Martínez, J. Guerra, I. Posadas and V. Ceña, *Pharm. Res.*, 2011, **28**, 1843–1858.
3 R. Kanasty, J. R. Dorkin, A. Vegas and D. Anderson, *Nat. Mater.*, 2013, **12**, 967–977.
4 J. E. Dahlman, C. Barnes, O. F. Khan, A. Thiriot, S. Jhunjunwala, T. E. Shaw, Y. Xing, H. B. Sager, G. Sahay, L. Speciner, A. Bader, R. L. Bogorad, H. Yin, T. Racie, Y. Dong, S. Jiang, D. Seedorf, A. Dave, K. Singh Sandhu, M. J. Webber, T. Novobrantseva, V. M. Ruda, K. R. Lytton-JeanAbigail, C. G. Levins, B. Kalish, D. K. Mudge, M. Perez, L. Abezgauz, P. Dutta, L. Smith, K. Charisse, M. W. Kieran, K. Fitzgerald, M. Nahrendorf, D. Danino, R. M. Tuder, U. H. von Andrian, A. Akinc, D. Panigrahy, A. Schroeder, V. Koteliansky, R. Langer and D. G. Anderson, *Nat. Nanotechnol.*, 2014, **9**, 648–655.
5 M. L. Chen, S. Gao, M. D. Dong, J. Song, C. X. Yang, K. A. Howard, J. Kjems and F. Besenbacher, *ACS Nano*, 2012, **6**, 4835–4844.
6 H. Lee, A. K. R. Lytton-Jean, Y. Chen, K. T. Love, A. I. Park, E. D. Karagiannis, A. Sehgal, W. Querbes, C. S. Zurenko, M. Jayaraman, C. G. Peng, K. Charisse, A. Borodovsky, M. Manoharan, J. S. Donahoe, J. Truelove, M. Nahrendorf, R. Langer and D. G. Anderson, *Nat. Nanotechnol.*, 2012, **7**, 389–393.
7 A.-M. Caminade, C.-O. Turrin and J.-P. Majoral, *Chem. – Eur. J.*, 2008, **14**, 7422–7432.
8 I. Posadas, F. J. Guerra and V. Ceña, *Nanomedicine*, 2010, **5**, 1219–1236.
9 O. F. Khan, E. W. Zaia, S. Jhunjhunwala, W. Xue, W. Cai, D. S. Yun, C. M. Barnes, J. E. Dahlman, Y. Dong, J. M. Pelet, M. J. Webber, J. K. Tsosie, T. E. Jacks, R. Langer and D. G. Anderson, *Nano Lett.*, 2015, **15**, 3008–3016.
10 D. A. Tomalia, H. Baker, J. Dewald, M. Hall, G. Kallos, S. Martin, J. Roeck, J. Ryder and P. Smith, *Polym. J.*, 1985, **17**, 117–132.
11 M. K. Mishra, C. A. Beaty, W. G. Lesniak, S. P. Kambhampati, F. Zhang, M. A. Wilson, M. E. Blue, J. C. Troncoso, S. Kannan, M. V. Johnston, W. A. Baumgartner and R. M. Kannan, *ACS Nano*, 2014, **8**, 2134–2147.
12 G. M. Pavan, S. Monteagudo, J. Guerra, B. Carrion, V. Ocana, J. Rodriguez-Lopez, A. Danani, F. C. Perez-Martinez and V. Ceña, *Curr. Med. Chem.*, 2012, **19**, 4929–4941.
13 F. Rico and V. T. Moy, *J. Mol. Recognit.*, 2007, **20**, 495–501.
14 V. T. Moy, E. L. Florin and H. E. Gaub, *Science*, 1994, **266**, 257–259.
15 A. R. Bizzarri and S. Cannistraro, *Nanotechnology*, 2014, **25**, 335102.
16 P. Hinterdorfer, W. Baumgartner, H. J. Gruber, K. Schilcher and H. Schindler, *Proc. Natl. Acad. Sci. U. S. A.*, 1996, **93**, 3477–3481.
17 J. Preiner, N. S. Losilla, A. Ebner, P. Annibale, F. Biscarini, R. Garcia and P. Hinterdorfer, *Nano Lett.*, 2009, **9**, 571–575.
18 S. Casalini, A. C. Dumitru, F. Leonardi, C. A. Bortolotti, E. T. Herruzo, A. Campana, R. F. de Oliveira, T. Cramer, R. Garcia and F. Biscarini, *ACS Nano*, 2015, **9**, 5051–5062.
19 F. Klingberg, M. L. Chow, A. Koehler, S. Boo, L. Buscemi, T. M. Quinn, M. Costell, B. A. Alman, E. Genot and B. Hinz, *J. Cell Biol.*, 2014, **207**, 283–297.
20 M. Carrion-Vazquez, A. F. Oberhauser, S. B. Fowler, P. E. Marszalek, S. E. Broedel, J. Clarke and J. M. Fernandez, *Proc. Natl. Acad. Sci. U. S. A.*, 1999, **96**, 3694–3699.
21 R. Petrosyan, C. A. Bippes, S. Walheim, D. Harder, D. Fotiadis, T. Schimmel, D. Alsteens and D. J. Müller, *Nano Lett.*, 2015, **15**, 3624–3633.
22 F. Rico, L. Gonzalez, I. Casuso, M. Puig-Vidal and S. Scheuring, *Science*, 2013, **342**, 741–743.
23 M. Rief, M. Gautel, F. Oesterhelt, J. M. Fernandez and H. E. Gaub, *Science*, 1997, **276**, 1109–1112.
24 C. Tromas, J. Rojo, J. M. de la Fuente, A. G. Barrientos, R. García and S. Penadés, *Angew. Chem., Int. Ed.*, 2001, **40**, 3052–3055.

25 R. M. A. Sullan, A. Beaussart, P. Tripathi, S. Derclaye, S. El-Kirat-Chatel, J. K. Li, Y.-J. Schneider, J. Vanderleyden, S. Lebeer and Y. F. Dufrene, *Nanoscale*, 2014, **6**, 1134–1143.
26 J. Beckmann, R. Schubert, R. Chiquet-Ehrismann and D. J. Müller, *Nano Lett.*, 2013, **13**, 2937–2946.
27 R. Merkel, P. Nassoy, A. Leung, K. Ritchie and E. Evans, *Nature*, 1999, **397**, 50–53.
28 E. Evans and K. Ritchie, *Biophys. J.*, 1997, **72**, 1541–1555.
29 A. Noy and R. W. Friddle, *Methods*, 2013, **60**, 142–150.
30 I. D. Medalsy and D. J. Müller, *ACS Nano*, 2013, **7**, 2642–2650.
31 S. Xu, M. D. Dong, X. Liu, K. A. Howard, J. Kjems and F. Besenbacher, *Biophys. J.*, 2007, **93**, 952–959.
32 S. Sadekar and H. Ghandehari, *Adv. Drug Delivery Rev.*, 2012, **64**, 571–588.
33 I. Posadas, F. C. Pérez-Martínez, J. Guerra, P. Sánchez-Verdú and V. Ceña, *J. Neurochem.*, 2012, **120**, 515–527.
34 M. D. Pérez-Carrión, F. C. Pérez-Martínez, S. Merino, P. Sánchez-Verdú, J. Martínez-Hernández, R. Luján and V. Ceña, *J. Neurochem.*, 2012, **120**, 259–268.
35 A. C. Rodrigo, I. Rivilla, F. C. Pérez-Martínez, S. Monteagudo, V. Ocaña, J. Guerra, J. C. García-Martínez, S. Merino, P. Sánchez-Verdú, V. Ceña and J. Rodríguez-López, *Biomacromolecules*, 2011, **12**, 1205–1213.
36 A. C. Dumitru, F. M. Espinosa, R. Garcia, G. Foschi, S. Tortorella, F. Valle, M. Dallavalle, F. Zerbetto and F. Biscarini, *Nanoscale*, 2015, **7**, 5403–5410.
37 A. Fuhrmann, J. C. Schoening, D. Anselmetti, D. Staiger and R. Ros, *Biophys. J.*, 2009, **96**, 5030–5039.
38 J. Hutter and J. Bechhoefer, *Rev. Sci. Instrum.*, 1993, **64**, 1868–1873.
39 H. J. Butt and M. Jaschke, *Nanotechnology*, 1995, **6**, 1.
40 C. Guo, B. Wang, L. Wang and B. Xu, *Chem. Commun.*, 2012, **48**, 12222–12224.
41 O. E. Farrance, E. Paci, S. E. Radford and D. J. Brockwell, *ACS Nano*, 2015, **9**, 1315–1324.
42 L. Buscemi, D. Ramonet, F. Klingberg, A. Formey, J. Smith-Clerc, J.-J. Meister and B. Hinz, *Curr. Biol.*, 2011, **21**, 2046–2054.
43 S. Guo, C. Ray, A. Kirkpatrick, N. Lad and B. B. Akhremitchev, *Biophys. J.*, 2008, **95**, 3964–3976.
44 P. Kebbekus, D. E. Draper and P. Hagerman, *Biochemistry*, 1995, **34**, 4354–4357.
45 J. A. Abels, F. Moreno-Herrero, T. van der Heijden, C. Dekker and N. H. Dekker, *Biophys. J.*, 2005, **88**, 2737–2744.
46 D. L. Nelson and M. M. Cox, *Lehninger Principles of Biochemistry*, W.H. Freeman & Company, New York, 5th edn, 2004.
47 P. J. Flory, *Statistical mechanics of chain molecules*, Interscience Publishers, 1969.
48 F. Oesterhelt, M. Rief and H. E. Gaub, *New J. Phys.*, 1999, **1**, 6.1–6.5.
49 T. V. Ratto, K. C. Langry, R. E. Rudd, R. L. Balhorn, M. J. Allen and M. W. McElfresh, *Biophys. J.*, 2004, **86**, 2430–2437.
50 C. Ray and B. B. Akhremitchev, *J. Am. Chem. Soc.*, 2005, **127**, 14739–14744.
51 T. A. Sulchek, R. W. Friddle, K. Langry, E. Y. Lau, H. Albrecht, T. V. Ratto, S. J. DeNardo, M. E. Colvin and A. Noy, *Proc. Natl. Acad. Sci. U. S. A.*, 2005, **102**, 16638–16643.
52 A. R. Bizzarri and S. Cannistraro, *Dynamic Force Spectroscopy and Biomolecular Recognition*, Taylor & Francis, 2012.
53 G. I. Bell, *Science*, 1978, **200**, 618–627.
54 E. A. Evans and D. A. Calderwood, *Science*, 2007, **316**, 1148–1153.
55 C. Friedsam, A. K. Wehle, F. Kühner and H. E. Gaub, *J. Phys.: Condens. Matter*, 2003, **15**, S1709.
56 H. Eyring, *J. Chem. Phys.*, 1935, **3**, 107–115.